Research Article | Vol. 26, No. 17 | 20 Aug 2018 | OPTICS EXPRESS 22536
Optics EXPRESS

Analytical mode normalization and resonant state expansion for bound and leaky modes in optical fibers - an efficient tool to model transverse disorder

S. Upendar,[1] I. Allayarov,[1] M. A. Schmidt,[2,3] and T. Weiss[1]

[1] *4th Physics Institute and Research Center SCoPE, University of Stuttgart, Pfaffenwaldring 57, 70569 Stuttgart, Germany*
[2] *Leibniz Institute of Photonic Technology e.V. Albert-Einstein-Str. 9, 07745 Jena, Germany*
[3] *Otto Schott Institute of Material Research, Friedrich Schiller University, Faunhoferstr. 6, 07743 Jena, Germany*
[*] *s.upendar@pi4.uni-stuttgart.de*

Abstract: We adapt the resonant state expansion to optical fibers such as capillary and photonic crystal fibers. As a key requirement of the resonant state expansion and any related perturbative approach, we derive the correct analytical normalization for all modes of these fiber structures, including leaky modes that radiate energy perpendicular to the direction of propagation and have fields that grow with distance from the fiber core. Based on the normalized fiber modes, an eigenvalue equation is derived that allows for calculating the influence of small and large perturbations such as structural disorder on the guiding properties. This is demonstrated for two test systems: a capillary fiber and a photonic crystal fiber.

OCIS codes: (060.5295) Photonic crystal fibers; (060.4005) Micro structured fibers; (080.1753) Computation methods.

References and links

1. P. St. J. Russell, "Photonic crystal fibers," Science **299**, 358–362 (2003).
2. J. C. Knight, J. Arriaga, T. A. Birks, A. Ortigosa-Blanch, W. J. Wadsworth, and P. St. J. Russell, "Anomalous dispersion in photonic crystal fiber," IEEE Photonics Technol. Lett. **12**, 807–809 (2000).
3. J. C. Knight, T. A. Birks, P. St. J. Russell, and D. M. Atkin, "All-silica single-mode optical fiber with photonic crystal cladding," Opt. Lett. **21**, 1547–1549 (1996).
4. T. Ritari, J. Tuominen, H. Ludvigsen, J. C. Petersen, T. Sørensen, T. P. Hansen, and H. R. Simonsen, "Gas sensing using air-guiding photonic bandgap fibers," Opt. Express **12**, 4080–4087 (2004).
5. J. M. Dudley, G. Genty, and S. Coen, "Supercontinuum generation in photonic crystal fiber," Rev. Mod. Phys. **78**, 1135 (2006).
6. F. Poli, A. Cucinotta, and S. Selleri, *Photonic Crystal Fibers: Properties and Applications* (Springer Science & Business Media, 2007).
7. G. Humbert, J. C. Knight, G. Bouwmans, P. St. J. Russell, D. P. Williams, P. J. Roberts, and B. J. Mangan, "Hollow core photonic crystal fibers for beam delivery," Opt. Express **12**, 1477–1484 (2004).
8. F. Benabid, J. C. Knight, G. Antonopoulos, and P. St. J. Russell, "Stimulated Raman scattering in hydrogen-filled hollow-core photonic crystal fiber," Science **298**, 399–402 (2002).
9. G. Li, M. Zeisberger, and M. A. Schmidt, "Guiding light in a water core all-solid cladding photonic band gap fiber–an innovative platform for fiber-based optofluidics," Opt. Express **25**, 22467–22479 (2017).
10. N. Granzow, P. Uebel, M. A. Schmidt, A. S. Tverjanovich, L. Wondraczek, and P. St. J. Russell "Bandgap guidance in hybrid chalcogenide–silica photonic crystal fibers," Opt. Lett. **36**, 2432–2434 (2011).
11. M. A. Schmidt, N. Granzow, N. Da, M. Peng, L. Wondraczek, and P. St. J. Russell "All-solid bandgap guiding in tellurite-filled silica photonic crystal fibers," Opt. Lett. **34**, 1946–1948 (2009).
12. M. H. Frosz, J. Nold, T. Weiss, A. Stefani, F. Babic, S. Rammler, and P. St. J. Russell, "Five-ring hollow-core photonic crystal fiber with 1.8 dB/km loss," Opt. Lett. **38**, 2215–2217 (2013).
13. Y. Wang, X. Zhang, X. Ren, L. Zheng, X. Liu, and Y. Huang, "Design and analysis of a dispersion flattened and highly nonlinear photonic crystal fiber with ultralow confinement loss," Appl. Opt. **49**, 292–297 (2010).
14. D. Nau, A. Schönhardt, C. Bauer, A. Christ, T. Zentgraf, J. Kuhl, and H. Giessen, "Disorder issues in metallic photonic crystals," Phys. Status Solidi B **243**, 2331–2343 (2006).
15. M. B. Doost, W. Langbein, and E. A. Muljarov, "Resonant-state expansion applied to three-dimensional open optical systems," Phys. Rev. A **90**, 013834 (2014).

#335079 https://doi.org/10.1364/OE.26.022536
Journal © 2018 Received 14 Jun 2018; revised 2 Aug 2018; accepted 3 Aug 2018; published 17 Aug 2018

Optics EXPRESS

16. E. A. Muljarov, W. Langbein, and R. Zimmermann, "Brillouin-Wigner perturbation theory in open electromagnetic systems," Europhys. Lett. **92**, 50010 (2010).
17. M. B. Doost, W. Langbein, and E. A. Muljarov, "Resonant state expansion applied to two-dimensional open optical systems," Phys. Rev. A **87**, 043827 (2013).
18. E. A. Muljarov and W. Langbein, "Exact mode volume and Purcell factor of open optical systems," Phys. Rev. B **94**, 235438 (2016).
19. L. J. Armitage, M. B. Doost, W. Langbein, and E. A. Muljarov, "Resonant-state expansion applied to planar waveguides," Phys. Rev. A **89**, 053832 (2014).
20. S. V. Lobanov, G. Zoriniants, W. Langbein, and E. A. Muljarov, "Resonant-state expansion of light propagation in nonuniform waveguides," Phys. Rev. A **95**, 053848 (2017).
21. C. Sauvan, J. P. Hugonin, I. S. Maksymov, and P. Lalanne, "Theory of the spontaneous optical emission of nanosize photonic and plasmon resonators," Phys. Rev. Lett. **110**, 237401 (2013).
22. P. T. Kristensen and S. Hughes, "Modes and mode volumes of leaky optical cavities and plasmonic nanoresonators," ACS Photonics **1**, 2–10 (2013).
23. R. Sammut and A. W. Snyder, "Leaky modes on circular optical waveguides," Appl. Opt. **15**, 477–482 (1976).
24. A. W. Snyder and J. D. Love, *Optical Waveguide Theory* (Chapman and Hall, 1983).
25. D. Marcuse, *Theory of Dielectric Optical Waveguides* (Academic, 1974).
26. S.-L. Lee, Y. Chung, L. A. Coldren, and N. Dagli, "On leaky mode approximations for modal expansion in multilayer open waveguides," IEEE J. Quantum Electron. **31**, 1790–1802 (1995).
27. H. M. Lai, P. T. Leung, K. Young, P. W. Barber, and S. C. Hill, "Time-independent perturbation for leaking electromagnetic modes in open systems with application to resonances in microdroplets," Phys. Rev. A **41**, 5187 (1990).
28. R. Sammut and A. W. Snyder, "Leaky modes on a dielectric waveguide: orthogonality and excitation," Appl. Opt. **15**, 1040–1044 (1976).
29. T. A. Birks, J. C. Knight, and P. St. J. Russell, "Endlessly single-mode photonic crystal fiber," Opt. Lett. **22**, 961–963 (1997).
30. E. A. Muljarov and T. Weiss, "Resonant-state expansion for open optical systems: generalization to magnetic, chiral, and bi-anisotropic materials," Opt. Lett. **43**, 1978–1981 (2018).
31. C.-T. Tai, *Dyadic Green Functions in Electromagnetic Theory* (IEEE, 1994).
32. T. Weiss, M. Mesch, M. Schäferling, H. Giessen, W. Langbein, and E. A. Muljarov, "From dark to bright: first-order perturbation theory with analytical mode normalization for plasmonic nanoantenna arrays applied to refractive index sensing," Phys. Rev. Lett. **116**, 237401 (2016).
33. E. A. Muljarov and W. Langbein, "Resonant-state expansion of dispersive open optical systems: Creating gold from sand," Phys. Rev. B **93**, 075417 (2016).
34. M. B. Doost, W. Langbein, and E. A. Muljarov, "Resonant-state expansion applied to planar open optical systems," Phys. Rev. A **85**, 023835 (2012).
35. G. B. Arfken and H. J. Weber, *Mathematical Methods for Physicists* (Academic Press, 1972).
36. T. Weiss, M. Schäferling, H. Giessen, N. A. Gippius, S. G. Tikhodeev, W. Langbein, and E. A. Muljarov, "Analytical normalization of resonant states in photonic crystal slabs and periodic arrays of nanoantennas at oblique incidence," Phys. Rev. B **96**, 045129 (2017).
37. J. D. Jackson, *Classical Electrodynamics* (Wiley, 1999).
38. E. A. Marcatili and R. A. Schmeltzer, "Hollow metallic and dielectric waveguides for long distance optical transmission and lasers," Bell Labs Tech. J. **43**, 1783-1809 (1964).
39. B. T. Kuhlmey, "Computer code CUDOS MOF Utilities," available at http://www.physics.usyd.edu.au/cudos/mofsoftware/index.html.
40. B. T. Kuhlmey, T. P. White, G. Renversez, D. Maystre, L. C. Botten, C. M. de Sterke, and R. C. McPhedran, "Multipole method for microstructured optical fibers. II. Implementation and results," J. Opt. Soc. Am. B **19**, 2331–2340 (2002).
41. T. P. White, B. T. Kuhlmey, R. C. McPhedran, D. Maystre, G. Renversez, C. M. de Sterke, and L. C. Botten, "Multipole method for microstructured optical fibers. I. Formulation," J. Opt. Soc. Am. B **19**, 2322–2330 (2002).
42. J. M. Fini, "Improved symmetry analysis of many-moded microstructure optical fibers," J. Opt. Soc. Am. B **21**, 1431–1436 (2004).

1. Introduction

Photonic crystal fibers guide light in a central defect core surrounded by a periodic cladding [1]. The guiding mechanism of the photonic crystal fiber can be a bandgap effect or modified total internal reflection in cases where the index of the core is larger than the effective cladding index. These fibers feature a high degree of light confinement, highly tunable dispersion properties [2], and single mode operation [3]. Photonic crystal fibers are extensively used in gas sensing [4], nonlinear optics such as supercontinuum generation [5], and many more applications [6–11].

In theoretical investigations, an ideal cladding is usually used to analyze such structures,

Optics EXPRESS

while a fabricated photonic crystal fiber cladding is never truly perfect [12, 13]. The fabrication process itself gives rise to shape and position disorders that influence the guiding properties. Studying that influence requires investigating many realizations [14], which is rather tedious in conventional numerical approaches. In contrast, the resonant state expansion has proven rather efficient for investigating a large set of similar three-dimensional resonator systems [15–18] and slab waveguides [19, 20]. The resonant state expansion is a rigorous perturbative approach, in which the resonant states (also known as quasi-normal modes [21, 22]) of a reference system (calculated either analytically or numerically) are used to set up an eigenvalue equation that provides the resonant states of a perturbed system. Here, we adapt the resonant state expansion to fiber geometries, in which the core and cladding modes constitute the resonant states, and treat disorder as a perturbation of the perfect cladding system.

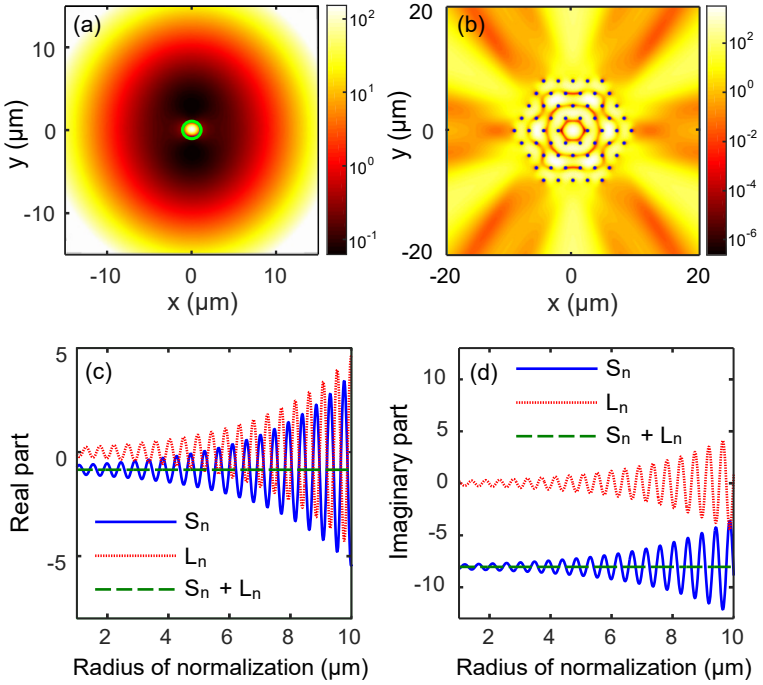

Fig. 1. (a) Axial component of the time-averaged Poynting vector of the fundamental core mode of a step index fiber with refractive indices of 1 and 1.44 in the core and cladding region, respectively, and a core radius of 1 μm (core region indicated by the green solid line) at a wavelength of 1 μm. (b) Axial component of the time-averaged Poynting vector for a higher-order core mode of a silica-air photonic crystal fiber with four rings of air holes of radius 0.25 μm and pitch 2.3 μm around a single-defect core. The refractive index of silica is taken as 1.44. The considered wavelength is 1 μm. Both modes in (a) and (b) exhibit fields that grow in the exterior with distance from the core. The bottom panels depict the real (c) and imaginary (d) parts of the surface term (blue solid line) and line term (red dotted line) of the normalization Eq. (8) as a function of the radius of normalization. Evidently, the divergence of the fields is manifested in the surface and line terms, while it is countervailed in their sum as the normalization constant.

As in any perturbation theory, the key factor in the resonant state expansion is the normalization of the resonant states. The normalization is not trivial, since the solutions of Maxwell's equations include leaky modes [23]. These modes radiate energy perpendicular to the fiber axis and have fields that grow with distance from the fiber core. This is displayed in Fig. 1 for a capillary fiber with air core and silica cladding (a) and a photonic crystal fiber with air inclusions and silica

Optics EXPRESS

background (b). A lot of work has been devoted to the normalization of leaky modes [24–27]. The most sophisticated approach is introducing a complex coordinate transformation in the exterior that suppresses the growth [28], which is equivalent to using perfectly matched layers and extending the area of normalization to the perfectly matched layers [21]. In contrast, we derive here an analytical normalization that can be calculated without any perfectly matched layers and is valid for both guided as well as leaky modes. Our new normalization can be easily applied when using standard numerical methods for the calculation of modes.

Here, the properties of the resonant state expansion with our analytical mode normalization is demonstrated for two fiber geometries. In the first example, we use the analytical solutions for a capillary fiber as basis to model the influence of a homogeneous change of the refractive index of the fiber core on the propagation constants of the fiber modes. In the second example, we investigate the influence of diameter disorder on the modal properties of a photonic crystal fiber [29].

2. Theory

In Gaussian units, the curl Maxwell's equations can be summarized in real space and frequency domain with time dependence $\exp(-i\omega t)$ by the compact operator form [30]

$$\underbrace{\begin{pmatrix} k_0\varepsilon & -\nabla\times \\ -\nabla\times & k_0\mu \end{pmatrix}}_{\equiv \mathbb{M}_0} \underbrace{\begin{pmatrix} \mathbf{E} \\ i\mathbf{H} \end{pmatrix}}_{\equiv \mathbb{F}} = \underbrace{\begin{pmatrix} \mathbf{J}_E \\ i\mathbf{J}_H \end{pmatrix}}_{\equiv \mathbb{J}}, \tag{1}$$

with electric and magnetic fields $\mathbf{E}$ and $\mathbf{H}$, respectively, permittivity and permeability tensors ε and μ, respectively, and $k_0 = \omega/c$. The right-hand side contains the electric source term $\mathbf{J}_E = -4\pi i\mathbf{j}/c$ with current density $\mathbf{j}$, and the magnetic source term $\mathbf{J}_H$ that has been introduced for the sake of symmetry.

For optical fibers, the permittivity and permeability tensors are translationally symmetric along the direction of propagation, which we choose as the z direction of our coordinate system. Defining the Fourier transform in this direction as

$$\hat{f}(\mathbf{r}_\parallel;\beta) = \frac{1}{2\pi}\int_{-\infty}^{\infty} \mathrm{d}z f(\mathbf{r}_\parallel;z)e^{-i\beta z}, \tag{2}$$

with $\mathbf{r}_{||}$ being the projection of $\mathbf{r}$ to the xy plane and the hat denoting Fourier transformed quantities, the Fourier transform of Eq. (1) yields

$$\begin{pmatrix} k_0\varepsilon & -\hat{\nabla}_\beta\times \\ -\hat{\nabla}_\beta\times & k_0\mu \end{pmatrix} \begin{pmatrix} \hat{\mathbf{E}} \\ i\hat{\mathbf{H}} \end{pmatrix} = \begin{pmatrix} \hat{\mathbf{J}}_E \\ i\hat{\mathbf{J}}_H \end{pmatrix}, \quad \text{with} \quad \hat{\nabla}_\beta \equiv \begin{pmatrix} \partial_x \\ \partial_y \\ i\beta \end{pmatrix}. \tag{3}$$

The Green's dyadic [31] of Eq. (3) satisfies the relation

$$\hat{\mathbb{M}}_0(\mathbf{r}_\parallel;\beta)\hat{\mathbb{G}}(\mathbf{r}_\parallel,\mathbf{r}'_\parallel;\beta) = \mathbb{1}\delta(\mathbf{r}_\parallel - \mathbf{r}'_\parallel), \tag{4}$$

and provides the solutions $\hat{\mathbb{F}}$ of Eq. (3) for a given source $\hat{\mathbb{J}}$ as

$$\hat{\mathbb{F}}(\mathbf{r}_\parallel) = \int \mathrm{d}\mathbf{r}'_\parallel\ \hat{\mathbb{G}}(\mathbf{r}_\parallel,\mathbf{r}'_\parallel;\beta)\hat{\mathbb{J}}(\mathbf{r}'_\parallel). \tag{5}$$

The Green's dyadic can be expanded in terms of the resonant states [15–17, 30, 32–34], which are solutions of Eq. (3) in the absence of sources for outgoing boundary conditions with eigenvectors $\hat{\mathbb{F}}_n$ and eigenvalues β_n:

$$\hat{\mathbb{M}}_0(\mathbf{r}_{||};\beta_n)\hat{\mathbb{F}}_n = 0. \tag{6}$$

Optics EXPRESS

Using the Mittag-Leffler theorem [35] and the reciprocity principle [36], it follows that

$$\hat{\mathbb{G}}(\mathbf{r}_\parallel, \mathbf{r}'_\parallel; \beta) = -\sum_n \frac{\hat{\mathbb{F}}_n(\mathbf{r}_\parallel) \otimes \hat{\mathbb{F}}^{\mathrm{R}}_n(\mathbf{r}'_\parallel)}{2N_n(\beta - \beta_n)} + \Delta\hat{\mathbb{G}}_{\mathrm{cuts}}, \tag{7}$$

with $\otimes$ denoting the outer vector product, and N_n being the normalization constant in order to assign the appropriate weight to the resonant states, since Eq. (6) provides the resonant field distribtuions only up to a constant factor. The factor $-1/2$ has been introduced for later convenience. The superscript R denotes the reciprocal conjugate resonant state, which is a solution of Eq. (6) at $-\beta_n$. Note that Eq. (7) is only valid within the regions of spatial inhomogeneities of the fiber [36], where the leaky modes do not exhibit any growth. Furthermore, $\Delta\hat{\mathbb{G}}_{\mathrm{cuts}}$ denotes cut contributions due to branch cuts in the involved analytical functions. In the following, we will focus on the contribution of the resonant states, keeping in mind that we can treat the cut contributions in a similar manner in numerical calculations [17, 32].

The derivation of the normalization constant is described in detail in Appendix A. The resulting normalization can be split into two terms comprising of a surface and a line integral that are evaluated on a circle with radius R outside the region of inhomogeneities, which yields

$$N_n = S_n + L_n, \tag{8}$$

with the surface term

$$S_n = \int_0^R \rho \mathrm{d}\rho \int_0^{2\pi} \mathrm{d}\phi \, (\hat{E}_{n,\rho}\hat{H}_{n,\phi} - \hat{E}_{n,\phi}\hat{H}_{n,\rho}), \tag{9}$$

which is proportional to the integral over the z component of the real-valued Poynting vector, and the line term

$$L_n = \frac{\varepsilon\mu k_0^2 + \beta_n^2}{2\varkappa_n^4} \int_0^{2\pi} \mathrm{d}\phi \left(\hat{E}_{n,z} \frac{\partial \hat{H}_{n,z}}{\partial \phi} - \hat{H}_{n,z} \frac{\partial \hat{E}_{n,z}}{\partial \phi} \right)_R$$

$$+ \frac{k_0\beta_n R^2}{2\varkappa_n^4} \int_0^{2\pi} \mathrm{d}\phi \left\{ \mu \left[\left(\frac{\partial \hat{H}_{n,z}}{\partial \rho} \right)^2 - \rho \hat{H}_{n,z} \frac{\partial}{\partial \rho} \left(\frac{1}{\rho} \frac{\partial \hat{H}_{n,z}}{\partial \rho} \right) \right] + \varepsilon \left[\left(\frac{\partial \hat{E}_{n,z}}{\partial \rho} \right)^2 - \rho \hat{E}_{n,z} \frac{\partial}{\partial \rho} \left(\frac{1}{\rho} \frac{\partial \hat{E}_{n,z}}{\partial \rho} \right) \right] \right\}_R, \tag{10}$$

where the subscript R indicates that the integrand is evaluated at radius R, and

$$\varkappa_n^2 = \varepsilon\mu k_0^2 - \beta_n^2. \tag{11}$$

For bound modes, the resonant states decay outside the regions of spatial inhomogeneities, so that the line term vanishes in the limit of $R \to \infty$. This results in the rather well-known normalization of resonant states by the integral over the z component of the Poynting vector [28]. For leaky modes, both the line and the surface term diverge. However, their sum countervails this divergence, resulting in a normalization constant independent of the radius of normalization, see Fig. 1. Hence, it is possible to calculate the normalization constant for a small area surrounding the regions of spatial inhomogeneities, without the need of including perfectly matched layers [21] or, equivalently, complex coordinates [28]. Furthermore, it should be noted that this approach also simplifies the normalization of bound modes in numerical calculations, since it allows restricting the normalization integrals, and, thus, the computational domain, to a small area that includes the spatial inhomogeneities.

Optics EXPRESS

Using the normalization to gauge the correct weight of the resonances, it is possible to determine the resonant states of a perturbed system (denoted by subscript ν) with perturbation $\Delta\varepsilon$ and $\Delta\mu$ that exhibits the same translational symmetry as ε and μ and vanish outside the regions of spatial ingomogeneities. The Maxwell operator $\hat{\mathbb{M}}$ of the perturbed system can be separated into the operator $\hat{\mathbb{M}}_0$ of the unperturbed system and the deviation $\Delta\hat{\mathbb{M}}$ as $\hat{\mathbb{M}} = \hat{\mathbb{M}}_0 + \Delta\hat{\mathbb{M}}$, with

$$\Delta\hat{\mathbb{M}}(\mathbf{r}_\parallel) = \begin{pmatrix} k_0\Delta\varepsilon(\mathbf{r}_\parallel) & 0 \\ 0 & k_0\Delta\mu(\mathbf{r}_\parallel) \end{pmatrix}. \tag{12}$$

Thus, we can recast Eq. (6) in the form

$$\hat{\mathbb{M}}_0(\mathbf{r}_\parallel;\beta_\nu)\hat{\mathbb{F}}_\nu(\mathbf{r}_\parallel) = -\Delta\hat{\mathbb{M}}(\mathbf{r}_\parallel)\hat{\mathbb{F}}_\nu(\mathbf{r}_\parallel), \tag{13}$$

where $\hat{\mathbb{F}}_\nu$ is the resonant field distribution of a resonant state in the perturbed system with propagation constant β_ν. Using Eq. (5), we obtain

$$\hat{\mathbb{F}}_\nu(\mathbf{r}_\parallel) = -\int \mathrm{d}\mathbf{r}'_\parallel\ \hat{\mathbb{G}}(\mathbf{r}_\parallel,\mathbf{r}'_\parallel;\beta_\nu)\Delta\hat{\mathbb{M}}(\mathbf{r}'_\parallel)\hat{\mathbb{F}}_\nu(\mathbf{r}'_\parallel). \tag{14}$$

Next, we construct the resonant states of the perturbed system as a linear combination of the normalized resonant states of the unperturbed system:

$$\hat{\mathbb{F}}_\nu(\mathbf{r}_\parallel) = \sum_n b_n^{(\nu)}\hat{\mathbb{F}}_n(\mathbf{r}_\parallel), \tag{15}$$

Using this ansatz in Eq. (14) and equating it for each $\hat{\mathbb{F}}_n$ independently, we obtain

$$\beta_\nu b_n^{(\nu)} = \beta_n b_n^{(\nu)} + \frac{1}{2}\sum_{n'} V_{nn'} b_{n'}^{(\nu)}, \tag{16}$$

where

$$V_{nn'} = \int \mathrm{d}\mathbf{r}_\parallel\ \hat{\mathbb{F}}_n^{\mathrm{R}}(\mathbf{r}_\parallel)\cdot\Delta\mathbb{M}(\mathbf{r}_\parallel)\hat{\mathbb{F}}_{n'}(\mathbf{r}_\parallel). \tag{17}$$

The above equations describe a linear eigenvalue problem with β_ν as the eigenvalue. Note that the sum in Eq. (15) is carried out over all resonant states of the unperturbed system, but in real calculations, a truncated basis is used to expand $\hat{\mathbb{F}}_\nu$. The choice of the basis size has to be taken large enough to accurately account for the perturbations in the system.

It should be noted that the above equations are given in Gaussian units. However, their transformation to SI units is straight-forward: One simply has to replace the permittivity and permeability by the relative permittivity and permeability, and substitute $\mathbf{H}$ with $Z_0\mathbf{H}^{\mathrm{SI}}$ as well as $\mathbb{J}$ with $Z_0\mathbb{J}^{\mathrm{SI}}$, with $\mathbf{J}_E^{\mathrm{SI}} = -i\mathbf{j}^{\mathrm{SI}}$ and Z_0 as the vacuum impedance, while $\mathbf{E}$ has to be replaced by $\mathbf{E}^{\mathrm{SI}}$.

3. Results and discussion

We first consider as our unperturbed system a capillary fiber with core index 1 and cladding index 1.44 having a core radius of 8 μm. The values of the propagation constant, and hence, the effective index of the fundamental HE_{11} mode as well as those of higher-order modes have been determined analytically by solving their characteristic equation [24, 37, 38] at a wavelength of 1 μm. The fields of the fiber are proportional to Bessel functions inside the core and outgoing Hankel functions in the cladding region.

A homogeneous perturbation of Δn is introduced inside the core of the fiber changing the core index to $\mathrm{n_{core}}+\Delta n$. As our perturbation is azimuthally symmetric, we only require modes of the same symmetry as the fundamental core mode to set up our eigenvalue problem of Eq. (16). The

Optics EXPRESS

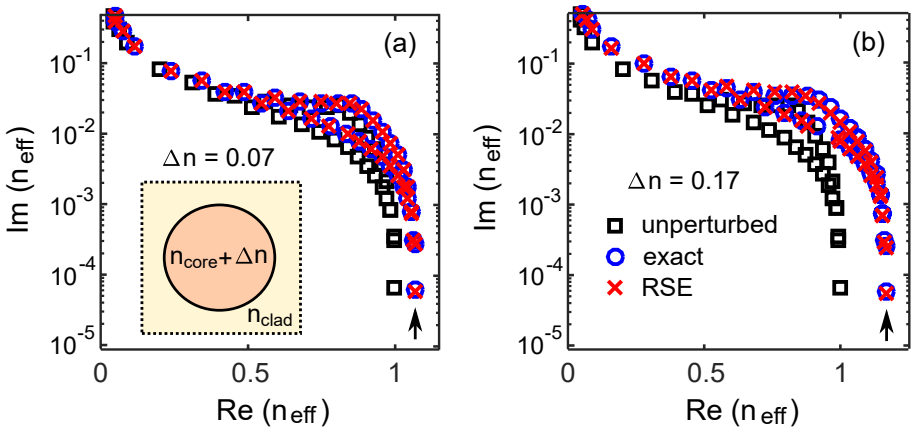

Fig. 2. Effective refractive indices of modes in a capillary fiber with a homogeneous perturbation in the core region of (a) $\Delta n = 0.07$ and (b) $\Delta n = 0.17$. The results from the resonant state expansion (red crosses) are compared with the exact analytical solution (blue circles) for the perturbed system at a wavelength of 1 μm. The unperturbed system has a core index of 1, cladding index of 1.44, and a radius of 8 μm, with its effective refractive indices denoted by black squares. The number of modes used is 154. The black arrow indicates the fundamental core mode.

comparison of the resonant state expansion with the exact analytical solution for the fundamental and higher order modes of azimuthal order $m = 1$ is shown in Fig. 2 for (a) $\Delta n = 0.07$ and (b) $\Delta n = 0.17$. We can see that there is a good agreement not only for the fundamental mode (indicated by the arrow) but also for the higher order modes of the system. The number of modes used is 154, with $|\mathrm{Re}(n_{\mathrm{eff}})|$ between 0.01279 and 0.9989 and pairs of modes symmetrically distributed on the complex β plane with propagation constants β_n and $-\beta_n$.

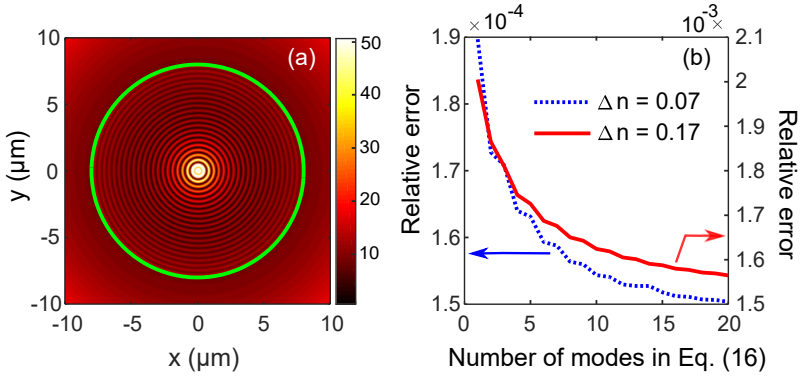

Fig. 3. (a) Spatial distribution of the time-averaged Poynting vector of a higher-order core mode supported by a capillary fiber with parameters as used in Fig. 2. The fiber core is indicated by the green solid line. The effective index of the unperturbed mode is 0.03139 + 1.0103i. (b) Relative error of the effective index of the higher-order mode with respect to the number of modes used in Eq. (16). Two refractive index differences have been considered as perturbations (dashed blue line: $\Delta n = 0.07$, solid red line: $\Delta n = 0.17$).

The relative error given by $|1 - n_{\mathrm{eff}}^{\mathrm{RSE}}/n_{\mathrm{eff}}^{\mathrm{exact}}|$ is displayed in Fig. 3 for a higher-order core mode ($n_{\mathrm{eff}} = 0.03139 + 1.0103i$ in the unperturbed fiber) and for two index differences ($\Delta n = 0.07$ and 0.17). It can be seen that the relative error decreases monotonously with increasing

Optics EXPRESS

number of basis states and reaches values on the order of 10^{-3} and 10^{-4} for 20 basis states. Note that the lowest relative error is achieved for the fundamental core mode, which is on the order of 10^{-6} for $\Delta n = 0.07$ and 20 basis states.

As a second example, we consider a silica-air photonic crystal fiber of air holes with radius $r_0 = 0.25$ μm in four cladding rings with pitch 2.3 μm around a single defect core. We numerically derive the modes of the photonic crystal fiber by the multipole method [39–42]. The solutions of the unperturbed fiber are then used as basis functions for the perturbed system, in which we introduce diameter disorder in each and every inclusion in the cladding region. The range of the diameter disorder is determined by the disorder parameter Δ as $r_0 \pm \Delta$. Within that radius range of width 2Δ, a uniform distribution of disorder is used. The probability density for a uniform distribution is given as,

$$f(r) = \begin{cases} \frac{1}{2\Delta} & \text{for } r_0 - \Delta \le r \le r_0 + \Delta \\ 0 & \text{for } r < r_0 - \Delta \text{ or } r > r_0 + \Delta \end{cases} \tag{18}$$

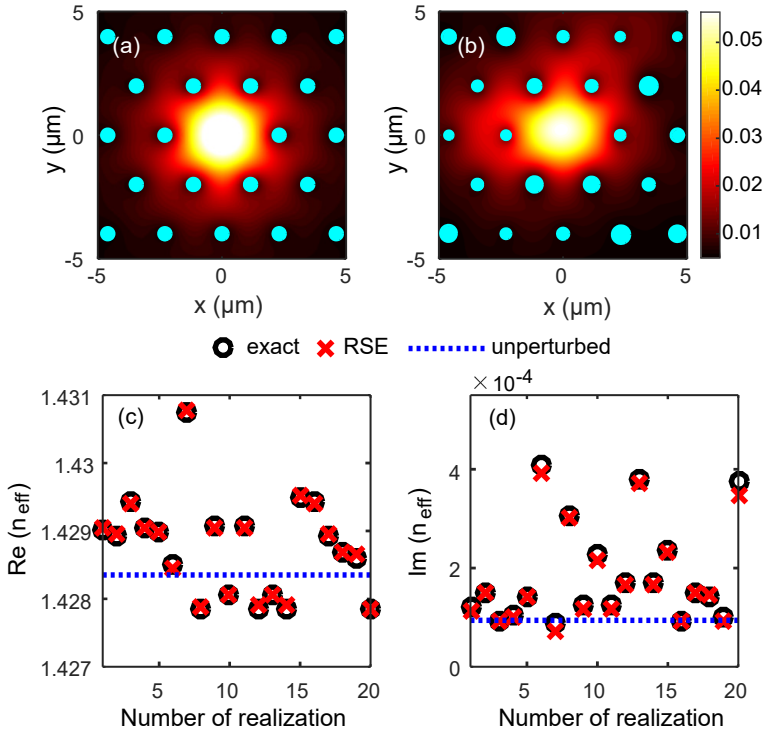

Fig. 4. Axial component of the time-averaged Poynting vector of the fundamental core mode of a silica-air photonic crystal fiber with diameter disorder for disorder parameter (a) Δ = 0 μm and (b) Δ = 0.1 μm. The disorder parameter provides the range of radii in the disordered fiber as $r_0 \pm \Delta$, with r_0 being the radius of the air holes in the ordered fiber. The geometrical parameters of the fiber are the same as in Fig. 1(b). Panels (c) and (d) show the comparison of the real and imaginary parts of the effective indices from the resonant state expansion (red crosses) with the exact numerical solution of the perturbed system (black circles) for 20 realizations of disorder at a wavelength of 1.55 μm. The number of modes used for the resonant state expansion is 190. The blue dotted line indicates the effective index for an unperturbed cladding.

We set up our eigenvalue problem with 190 modes (95 pairs of modes symmetrically distributed on the complex β plane) that have effective indices close to that of the fundamental mode. The

Optics EXPRESS

modes chosen for the eigenvalue problem exhibit all kinds of azimuthal symmetries, because the azimuthal symmetry is broken by the disorder. The comparison of the real and imaginary part of the effective index obtained from the resonant state expansion (red crosses) and full numerical calculations (black circles) can be seen in Fig. 4 (c) and (d), respectively, for 20 realizations and $\Delta = 0.1$ μm at a wavelength of 1.55 μm. Evidently, there is a good agreement between the two methods for the shown realizations. For the given photonic crystal fiber, the computational time for the simulation of a fiber mode by the multipole method is around 8 minutes on an i7-4790CPU@3.60 GHz desktop computer, while solving the eigenvalue Eq. (16) of the resonant state expansion takes 0.17 s.

In Fig. 5 (a) and (b), we display the real and imaginary parts of the effective index averaged over 200 realizations for disorder parameters ranging from $\Delta = 0$ to 0.11 μm. More specifically, we generate 200 sets of random numbers between 0 and 1 for each air hole and multiply them with different values of Δ in order to generate the disordered fibers. The standard deviation of the effective index is plotted as error bars that grow with increasing Δ. Interestingly, the average $\mathrm{Re}(n_{\mathrm{eff}})$ has a linear dependence with Δ while the $\mathrm{Im}(n_{\mathrm{eff}})$ exhibits a more quadratic behavior.

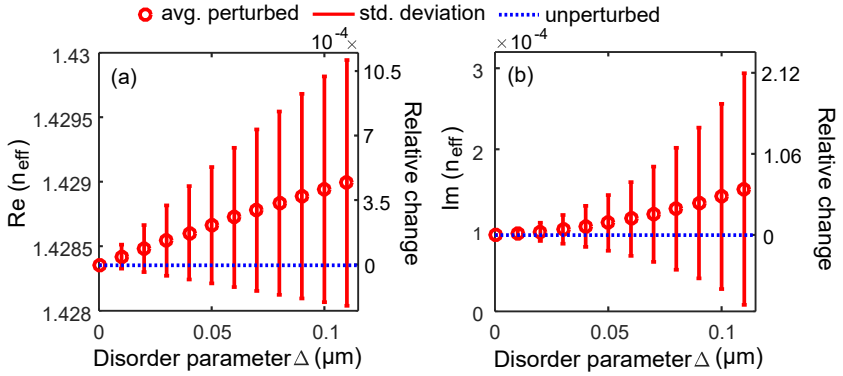

Fig. 5. Real (a) and imaginary (b) part of the effective index of the fundamental core mode as a function of the disorder parameter Δ averaged over 200 realizations of diameter disorder at a wavelength of 1.55 μm. The averaged real part grows almost linearly with increasing Δ, while the imaginary part is growing quadratically. The standard deviation is indicated by the errorbars. The blue dotted line indicates the effective index of the unperturbed cladding.

4. Conclusion

We have derived an analytical normalization for modes in fiber geometries that is valid not only for guided but also for leaky modes. We have shown that the normalization constant is independent of the radius of integration even for leaky modes with fields that grow with distance from the fiber core. Thus, it is possible to set up an eigenvalue equation that allows us to calculate the effective refractive indices of modes in a perturbed system. The accuracy of this so-called resonant state expansion has been demonstrated for capillary-type and photonic crystal fibers. For the latter, we have studied diameter disorder in the cladding of a silica-air photonic crystal fiber for different disorder parameters averaged over many realizations. Here, the resonant state expansion is clearly superior compared to full numerical simulations, since it does not require to repeatedly solve Maxwell's equations, while the numerical effort for solving the eigenvalue equation is rather low. Thus, it is possible to derive the influence of disorder on the guiding properties such as propagation constant and loss efficiently.

Optics EXPRESS

A. Normalization

Let us consider the Maxwell's equation with a source term that vanishes at resonance:

$$\hat{\mathbb{M}}_0(\mathbf{r}_\parallel;\beta)\hat{\mathbb{F}} = (\beta-\beta_n)\sigma_n(\mathbf{r}_\parallel). \tag{19}$$

Here, $\sigma_n(\mathbf{r}_\parallel)$ is chosen to vanish outside the region of spatial inhomogeneities. Taking the source term and convoluting with the Green's dyadic in the limit $\beta \to \beta_n$, we get

$$\hat{\mathbb{F}}_n(\mathbf{r}_\parallel) = \lim_{\beta\to\beta_n}\sum_{n'}\frac{-1}{2N_{n'}}\frac{\beta-\beta_n}{\beta-\beta_{n'}}\hat{\mathbb{F}}_{n'}(\mathbf{r}_\parallel)\int \mathrm{d}\mathbf{r}'_\parallel\ \hat{\mathbb{F}}^{\mathrm{R}}_{n'}(\mathbf{r}'_\parallel)\sigma_n(\mathbf{r}'_\parallel). \tag{20}$$

This can be only fulfilled for

$$\int \mathrm{d}\mathbf{r}'_\parallel\ \hat{\mathbb{F}}^{\mathrm{R}}_n(\mathbf{r}'_\parallel)\sigma_n(\mathbf{r}'_\parallel) = -2N_n. \tag{21}$$

To derive the normalization equation, we multiply Eq. (19) with $\hat{\mathbb{F}}^{\mathrm{R}}_n(\mathbf{r}_\parallel)$ and subtract a zero in the form of

$$0 = \hat{\mathbb{F}}(\mathbf{r}_\parallel;\beta)\cdot\hat{\mathbb{M}}_0(\mathbf{r}_\parallel;-\beta_n)\hat{\mathbb{F}}^{\mathrm{R}}_n(\mathbf{r}_\parallel), \tag{22}$$

to obtain,

$$\hat{\mathbb{F}}^{\mathrm{R}}_n(\mathbf{r}_\parallel)\cdot\hat{\mathbb{M}}_0(\mathbf{r}_\parallel;\beta)\hat{\mathbb{F}}(\mathbf{r}_\parallel;\beta) - \hat{\mathbb{F}}(\mathbf{r}_\parallel;\beta)\cdot\hat{\mathbb{M}}_0(\mathbf{r}_\parallel;-\beta_n)\hat{\mathbb{F}}^{\mathrm{R}}_n(\mathbf{r}_\parallel) = (\beta-\beta_n)\hat{\mathbb{F}}^{\mathrm{R}}_n(\mathbf{r}_\parallel)\cdot\sigma_n(\mathbf{r}_\parallel). \tag{23}$$

Dividing by $\beta-\beta_n$, integrating over the spatial inhomogeneities in the limit $\beta\to\beta_n$, and using that $\varepsilon^{\mathrm{T}} = \varepsilon$ as well as $\mu^{\mathrm{T}} = \mu$ for reciprocal systems, we get

$$\begin{aligned}-2N_n = \lim_{\beta\to\beta_n}\int \mathrm{d}\mathbf{r}_\parallel\ \frac{-i}{\beta-\beta_n}\nabla_\parallel\cdot[\hat{\mathbf{E}}(\mathbf{r}_\parallel;\beta)\times\hat{\mathbf{H}}^{\mathrm{R}}_n(\mathbf{r}_\parallel) - \hat{\mathbf{E}}^{\mathrm{R}}_n(\mathbf{r}_\parallel)\times\hat{\mathbf{H}}(\mathbf{r}_\parallel;\beta)]\\ + \int \mathrm{d}\mathbf{r}_\parallel\ [\hat{\mathbf{E}}_n(\mathbf{r}_\parallel)\times\hat{\mathbf{H}}^{\mathrm{R}}_n(\mathbf{r}_\parallel) - \hat{\mathbf{E}}^{\mathrm{R}}_n(\mathbf{r}_\parallel)\times\hat{\mathbf{H}}_n(\mathbf{r}_\parallel)]_z.\end{aligned} \tag{24}$$

The subscript z indicates the integration of the z component in the second term which results in the surface integral of Eq. (9) when using that, due to symmetry, the in-plane components of the electric field and the z component of the magnetic field of resonant states with eigenvalues β_n and $-\beta_n$ are identical, while we have to multiply all other components with -1 in order to convert $\hat{\mathbb{F}}^{\mathrm{R}}_n$ into $\hat{\mathbb{F}}_n$. The first term can be converted to a line integral by using the divergence theorem. The curve of integration is taken as a circle of radius R outside the region of inhomogeneities. For evaluating the limit $\beta\to\beta_n$, we carry out a Taylor expansion around β_n as

$$\hat{\mathbb{F}}(\mathbf{r}_\parallel;\beta) = \hat{\mathbb{F}}_n(\mathbf{r}_\parallel) + (\beta-\beta_n)\frac{\partial\hat{\mathbb{F}}(\mathbf{r}_\parallel;\beta)}{\partial\beta}\bigg|_{\beta_n} + \frac{(\beta-\beta_n)^2}{2}\frac{\partial^2\hat{\mathbb{F}}(\mathbf{r}_\parallel;\beta)}{\partial\beta^2}\bigg|_{\beta_n} + \dots, \tag{25}$$

which results in a line integral that contains $\hat{\mathbb{F}}^{\mathrm{R}}_n$ as well as first-order derivatives of $\hat{\mathbb{F}}$ with respect to β at β_n. Moreover, due to the aforementioned relations between $\hat{\mathbb{F}}^{\mathrm{R}}_n$ and $\hat{\mathbb{F}}_n$, we can rewrite Eq. (24) as

$$\begin{aligned}N_n = \frac{\beta_n R}{2i\varkappa_n}\int_0^{2\pi}\mathrm{d}\phi\ (\frac{\partial\hat{E}_{n,\phi}}{\partial\varkappa}\hat{H}_{n,z} + \frac{\partial\hat{E}_{n,z}}{\partial\varkappa}\hat{H}_{n,\phi} - \frac{\partial\hat{H}_{n,\phi}}{\partial\varkappa}\hat{E}_{n,z} - \frac{\partial\hat{H}_{n,z}}{\partial\varkappa}\hat{E}_{n,\phi})\\ + \int \mathrm{d}\mathbf{r}_\parallel\ (\hat{E}_{n,\rho}\hat{H}_{n,\phi} - \hat{E}_{n,\phi}\hat{H}_{n,\rho}).\end{aligned} \tag{26}$$

Optics EXPRESS

Note that we have converted the derivative with respect to β to a derivative with respect to $\varkappa$ by using the relation in Eq. (11). The derivative with respect to $\varkappa$ can then be converted to spatial derivatives by using the following relations:

$$\frac{\partial \hat{E}_z}{\partial \varkappa} = \frac{\rho}{\varkappa}\frac{\partial \hat{E}_z}{\partial \rho}, \qquad \frac{\partial \hat{H}_z}{\partial \varkappa} = \frac{\rho}{\varkappa}\frac{\partial \hat{H}_z}{\partial \rho}. \tag{27}$$

The $\hat{E}_\phi$ and $\hat{H}_\phi$ field components can be derived from the $\hat{E}_z$ and $\hat{H}_z$ field components as

$$\hat{E}_\phi = \frac{i\beta}{\varkappa^2\rho}\frac{\partial \hat{E}_z}{\partial \phi} - \frac{ik_0\mu}{\varkappa^2}\frac{\partial \hat{H}_z}{\partial \rho}, \qquad \hat{H}_\phi = \frac{i\beta}{\varkappa^2\rho}\frac{\partial \hat{H}_z}{\partial \phi} + \frac{ik_0\varepsilon}{\varkappa^2}\frac{\partial \hat{E}_z}{\partial \rho}, \tag{28}$$

and they can be differentiated with respect to $\varkappa$ by using the relations for $\hat{E}_z$ and $\hat{H}_z$ given in Eq. (27). Substituting in Eq. (26) $\hat{E}_\phi$ and $\hat{H}_\phi$ by Eq. (28) and using that

$$\int_0^{2\pi} \mathrm{d}\phi \, \frac{\partial f}{\partial \phi} g = -\int_0^{2\pi} \mathrm{d}\phi \, f \frac{\partial g}{\partial \phi}, \tag{29}$$

with f and g being components of $\hat{\mathbf{E}}_n$ and $\hat{\mathbf{H}}_n$, respectively, we arrive after some algebra at Eq. (10).

Funding

DFG SPP 1839; MWK Baden-Württemberg.